A Biodegradable and Cross-Linkable Multiblock Copolymer Consisting of Poly(propylene fumarate) and Poly(ϵ-caprolactone): Synthesis, Characterization, and Physical Properties

Shanfeng Wang, Lichun Lu, James A. Gruetzmacher, Bradford L. Currier, and Michael J. Yaszemski*

Tissue Engineering and Polymeric Biomaterials Laboratory, Department of Orthopedic Surgery, Department of Physiology and Biomedical Engineering, Mayo Clinic College of Medicine, 200 First Street SW, Rochester, Minnesota 55905

Received April 25, 2005; Revised Manuscript Received June 28, 2005

ABSTRACT: In an effort to develop various controllable biomaterials, a series of novel cross-linkable and biodegradable multiblock poly(propylene fumarate-*co*-caprolactone) [P(PF-*co*-CL)] copolymers have been synthesized via a three-step polycondensation of oligomeric polypropylene fumarate (PPF) with polycaprolactone (PCL) diols. The chemical structures of 15 copolymers with various PCL compositions and segment lengths were further characterized by FTIR, ^{1}H NMR, and ^{13}C NMR spectra. Their physical and rheological properties have been determined extensively. The composition dependences of various characteristic temperatures such as glass transition temperature T_g, melting temperature T_m, and thermal degradation temperature T_d were demonstrated using a phase diagram. Together with DSC results, polarized optical microscopical graphs of several copolymers with high PCL compositions show spherulite crystalline structure. Particularly a banded spherulite has been found for a copolymer with a PCL composition of 87% when it crystallizes at room temperature. When the PCL composition in these copolymers is lower than 70%, the copolymers are amorphous with a reduced T_g. This is critical for an enhanced rate of biodegradation. Because of the flexibility of PCL segments in the copolymers, P(PF-*co*-CL) can be either self-cross-linked or photocross-linked without using any cross-linker. The unentangled characteristics have been verified by the melt viscosity's molecular weight dependence and the master curves of storage modulus G' and loss modulus G''. The introduction of PCL into the copolymer chain enhances the solubility in toluene. Dilute solution viscometry shows the effect of microstructure in intrinsic viscosity while this effect is insignificant in melt viscosity. Therefore, the physical properties of such a copolymer can be modulated by the composition and segment length to satisfy the needs in a variety of tissue engineering applications such as bone, cartilage, and nerve tube regenerations.

Introduction

Diverse clinical needs for bone regeneration arise from resection of primary and metastatic tumors, bone loss after skeletal trauma, total arthroplasty with bone deficiency, spinal arthrodesis, and trabecular voids. Recently developed injectable materials have fulfilled many design criteria for these diverse orthopedic applications.[1,2] A promising candidate material of this type is poly(propylene fumarate) (PPF), an unsaturated linear polyester that can be modified or cross-linked through its fumarate double bonds.[3]

PPF can be cross-linked via radical polymerization with monomers of methyl methacrylate or *N*-vinylpyrrolidinone (NVP) and biodegradable macromers of PPF diacrylate or poly(ethylene glycol) diacrylate.[3] The curing time has ranged from 1 to 121 min, depending on the ratio of initiator, monomer or macromer, and PPF.[3] The maximum temperature during PPF cross-linking has been 48 °C, which is less than that for PMMA bone cement that may reach temperatures over 90 °C during polymerization.[3] PPF degrades by simple hydrolysis of the ester bonds, and the degradation time depends on polymer characteristics such as molecular weight, type of cross-linker, and cross-linking density.[3] Although many efforts have been made to explore the applications of PPF-based materials, there are still many important limitations of this material. The propylene glycol in each repeating unit provides only one free rotating carbon−carbon bond that contributes to the rigidity of the PPF polymer chain. In addition, a cross-linker is needed to form cross-linked PPF networks via redox initiation, which may lead to cytotoxicity associated with unreacted cross-linking monomers. On the basis of such unsaturated PPF component, a few block copolymers such as poly(propylene fumarate-*co*-ethylene glycol) [P(PF-*co*-EG)],[4] poly(propylene fumarate-*co*-sebacate)-*co*-poly(ethylene glycol) (PPFS-*co*-PEG),[5] and poly(2-methyl-1,4-phenylene fumarate)-*co*-(propylene fumarate) [P(MPF-*co*-PF)][6] have been synthesized to obtain various physical properties that their parent polymers cannot reach.

Poly(ϵ-caprolactone) (PCL) is an FDA-approved biodegradable polymer with excellent biocompatibility and flexibility. PCL has been recently studied as a potential material for a temporary joint spacer[7] and tissue-engineering skin.[8] A variety of copolymers based on PCL have been made to enhance the applications and cross-linking properties of such material.[9] Because of its semicrystalline and hydrophobic characteristics, diblock or triblock copolymers based on PCL also have attracted much attention in polymer science community.[10,11] Particularly, shape-memory properties have been revealed in the copolymer networks based on PCL soft crystallizable segment.[12] Recently we have developed a copolymer of PCL and fumarate segments, poly(caprolactone fumarate) (PCLF).[13] Because of the presence of

* Corresponding author: e-mail yaszemski.michael@mayo.edu, Tel (507) 284-2267.

10.1021/ma050884c CCC: $30.25
Published on Web 07/30/2005

Scheme 1

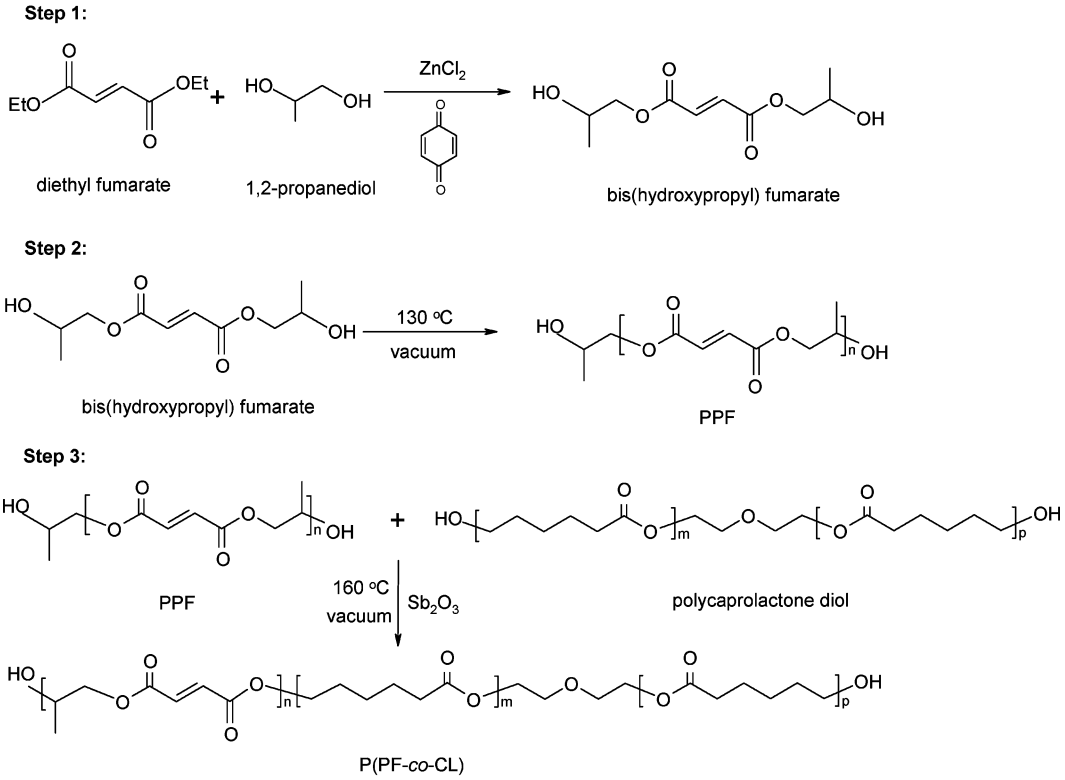

the PCL unit, the PCLF chain is much more flexible than the PPF chain. This renders PCLF self-cross-linkable without the use of any cross-linkers.[13] However, because the PCL segment is the dominating composition in PCLF, the double-bond density in the polymer chain is very low. The self-cross-linked PCLF network is therefore weak.

Here in this report we describe the synthesis, characterizations, and physical properties of a novel multiblock copolymer of P(PF-*co*-CL) that has desirable and controllable mechanical strength and self-cross-linking characteristics. The relative rigid unsaturated PPF segment provides mechanical strength and cross-linkability while the PCL segment provides flexibility for self-cross-linking. The physical, chemical, mechanical, and degradation properties of P(PF-*co*-CL) can be modulated by varying the PPF and PCL molecular weights and their block lengths. In addition, only PPF of relatively low molecular weights (M_w < 10 000 g mol^{-1}) have been synthesized due to heat-induced cross-linking during polymerization.[3i] For P(PF-*co*-CL), it is possible to achieve a higher molecular weight because the saturated component of PCL in the polymerization lessens the possibility of the cross-linking process of double bonds in PPF segments.

Experimental Section

Materials. PCL diols [α,ω-dihydroxy poly(ε-caprolactone)] with nominal molecular weights of 530, 1250, and 2000 g mol^{-1} were purchased from Aldrich Co. (Milwaukee, WI) and had a chemical structure as H−[O(CH$_2$)$_5$CO−]$_m$OCH$_2$CH$_2$−O−CH$_2$-CH$_2$O[−OC(CH$_2$)$_5$O]$_n$−H. Prior to copolymerization, a certain amount of PCL diol was dried overnight in a vacuum oven at 50 °C. All the other chemicals in the present study were also purchased from Aldrich Co.

Polymer Synthesis. PPF was produced as described previously.[3j] It is also depicted in Scheme 1 as steps 1 and 2. In the first step, 259 g of diethyl fumarate and 342 g of 1,2-propylene glycol were mixed together in a 2 L three-neck round-bottom flask with 0.33 g of hydroquinone as a cross-linking inhibitor and 2.04 g of zinc chloride as a catalyst. The transesterification reaction obtained the fumaric diester by heating at 100 °C for 1 h and then at 150 °C for 7 h. The byproduct ethanol was removed under nitrogen. In the second step, the intermediate was polycondensed to form the linear PPF with hydroxyl groups on both ends with the removal of propylene glycol. The molecular weight of PPF can be modulated by varying the polymerization time. Typically the polymerization was performed under vacuum first at 100 °C and then at 130 °C for 1 or 3 h. After making the PPF block, the reaction was stopped by shutting off the vacuum condition and oil bath. The three PPF samples in Table 1 were obtained without doing further copolymerization with PCL block.

To synthesize a copolymer, a certain amount of PCL diol and 0.2 g of antimony trioxide as a catalyst were added to the reaction vessel right after the synthesis of PPF block. After mixing completely under nitrogen at 100 °C for 30 min, the reaction temperature was then raised gradually to 160 °C, and a vacuum of 0 mmHg was applied. The copolymerization

Table 1. Different Design Parameters for Polymerization

run no.	nominal mol wt of PCL	reaction time (h)		PCL feed ratio (by wt)	PCL wt ratio determined by NMR
		PPF	copolymer		
1	530	1	5	0.31	0.30
2	530	3	5	0.32	0.31
3	530	1	10	0.32	
4	1250	1	5	0.30	0.32
5	1250	3	5	0.29	0.31
6	2000	1	5	0.31	0.32
7	2000	3	5	0.33	0.34
8	2000	1	5	0.45	0.46
9	2000	1	5	0.41	0.43
10	530	1	5	0.54	0.51
11	1250	1	5	0.56	0.54
12	2000	1	5	0.87	0.86
13	2000	1	5	0.81	0.80
14	2000	1	5	0.70	0.68
15	1250	1	5	0.77	0.75
16	2000	1	5	0.90	0.89

generally took 5 h, and 1,2-propylene glycol was removed. The resulting P(PF-*co*-CL) copolymer was then purified by dissolving in methylene chloride and first washed twice by acid (600 mL of 10 wt % hydrochloric acid for each time) to remove catalysts. It was then purified using distilled water and saturated brine. The organic phase was dried with magnesium sulfate, which was subsequently removed by vacuum filtration. The viscous solution of P(PF-*co*-CL) in methylene chloride obtained by rotary evaporation was precipitated in a large amount of diethyl ether. Methylene chloride and ether in the final precipitated copolymer were removed by rotary evaporation again followed by vacuum-drying. The final product of P(PF-*co*-CL) is a transparent, light yellow, viscous melt or a waxlike solid depending on if the PCL content is lower or higher than 70%, respectively.

Characterizations. Gel permeation chromatography (GPC) was used to determine the molecular weight and polydispersity of the polymers herein. The GPC was carried out with a Waters 717 Plus autosampler GPC system (Waters, Milford, MA) connected to a model 515 HPLC pump and model 2410 refractive index detector. Monodisperse polystyrene standards (Polysciences, Warrington, PA) with four molecular weights (474, 6690, 18 600, and 38 000 g mol^{-1}) were used to obtain a universal calibration curve, and this was then used to calculate the molecular weights of the polymers herein. Fourier transform infrared spectroscopy (FTIR) spectra were obtained on a Nicolet 550 spectrometer. All the polymers were analyzed using a zinc selenide ATR crystal. The resolution of the instrument was specified as 4 cm^{-1} at a wavenumber of 1000 cm^{-1}. Proton and carbon nuclear magnetic resonance (NMR) spectra were acquired on a Varian Mercury Plus NMR spectrometer (^1H = 400.1 MHz, ^{13}C = 100.6 MHz) using $CDCl_3$ (δ = 7.27 ppm) solutions containing TMS. Differential scanning calorimetry (DSC) was measured on a TA Instruments Q1000 differential scanning calorimeter at a heating rate of 10 °C/min in a nitrogen atmosphere. To keep the same thermal history, each sample was preheated from room temperature to 100 °C and cooled to −90 °C at a cooling rate of 5 °C/min. Then the DSC scan was recorded via heating from −90 to 100 °C. The amorphous structure of the copolymers and the crystalline form of three PCL samples were observed using a Zeiss Axioskop polarizing optical microscope (POM). Thermogravimetric analysis (TGA) was done using a TA Instruments Q500 thermal analyst. The TGA data were obtained in flowing nitrogen at a heating rate of 20 °C/min.

Rheological Measurements and Dilute Solution Viscometry. Linear viscoelastic properties of the polymers were measured by a dynamic mechanical spectrometer (AR2000 rheometer, TA Instruments) at frequencies (ω) ranging from 0.1 to 628.3 rad/s and at various temperatures between 0 and 100 °C. The oscillatory shear measurements were carried out using a 20 mm diameter parallel plate flow cell, and a geometry gap setting of 1.0 mm was used. A small strain (γ < 0.05) was always applied when the complex modulus $|G^*|$ was large, and no strain amplitudes were larger than 0.10. Dynamic shear experiments were performed to measure the storage and loss moduli G' and G'' of the polymers besides the zero-shear viscosity η_0. The steady-state shear viscosities at low shear rate were also measured, and the results are consistent with the dynamic viscosity at low frequencies.

Intrinsic viscosities of the polymers were measured in toluene at 30.0 ± 0.05 °C with a calibrated Cannon Ubbehlobe capillary viscometer (model 0C, Cannon Instrument Co.) in a water bath equipped with a Lauda ECO-Line immersion circulator (Brinkmann Co.). Toluene was distilled from CaH_2 before being used as the solvent. The solvent flow time was about 218.73 s. The initial concentrations of the copolymer solutions are in a range between 1.19 and 8.52 g dL^{-1} inversely related to the copolymer molecular weight.

Solubility and Density Determination. Approximately 30 mg of copolymer samples was placed in 3 mL of nine different solvents including water, methylene chloride, tetrahydrofuran, acetone, dimethylformamide, methanol, toluene, hexane, and diethyl ether. The solubility of the copolymers in those solvents was judged by the naked eye after 24 h at room temperature. The density of all the polymers synthesized here was measured at 20 °C in a weighed GPC vial by comparing with the same volume of distilled water, which has a density of 0.998 21 g mL^{-1}.[14] The densities of three PCL diols were the label values (1.073 g cm^{-3}) from Aldrich Co.

Results and Discussion

Polymer Synthesis and Molecular Characterization. Sixteen polymerization formulations are tabulated in Table 1. The design parameters are the molecular weight of PCL diols, reaction times for synthesizing PPF block (step 2 in Scheme 1) and the final copolymer (step 3 in Scheme 1), and the weight ratio of PCL in the copolymers. When the reaction time for step 3 was 10 h (run 3 in Table 1), cross-linking occurred and prohibited yielding a large amount of un-cross-linked copolymer **3**, although a small piece of sample was obtained after being filtered to determine the molecular weight. The feed ratios of PCL diol in Table 1 were calculated from the feed weights of diethyl fumarate and PCL diol in the various polymerization formulations. The final copolymer composition can be obtained from ^1H NMR spectra and will be discussed later. To make the feed ratio equal to the final copolymer composition, no unreacted PCL diol or PPF should be left after polymerization. To achieve this goal, PCL composition has lower and upper limits.

The lower limit of PCL composition in the resulting copolymer is also the minimum PCL feed ratio required to react with all the PPF precursors. It exists theoretically when there is only one PCL block with the maximum molecular weight of PPF in each copolymer chain. The upper limit of PCL composition occurs when PPF precursor chains are all end-capped by two PCL blocks to form a triblock-like copolymer. Therefore, the minimum and maximum PCL diol feed ratios (i.e., the PCL composition in the final copolymers) are decided by (1) the molecular weight of PCL diol, M_1; (2) the molecular weight of PPF precursor, M_2; and (3) the approximate maximum molecular weight of PPF when it reacts with itself, M_∞. Here we use the molecular weight of PPF7hr in Table 2 for M_∞. On the basis of the information about the molecular weights in Table 2, one can roughly outline the boundary feed ratios in Figure 1 for each polymerization using the equations $\phi_{min} = M_1/(M_\infty + M_1)$ and $\phi_{max} = 2M_1/(M_2 + 2M_1)$. Most PCL feed ratios used in the present study lie between the lower and upper limits to ensure there was little unreacted PPF or PCL diol in the final products. From Figure 1, it can be expected that a lower starting PPF molecular weight and a higher PCL diol molecular weight are liable to have a higher maximum PCL composition.

The extent of reaction was monitored by GPC and FTIR. As also reported for P(PF-*co*-EG),[4] the measured molecular weights of the starting PCL diols are significantly higher than the nominal values due to the fact that PS standard is used here. It can be seen in Figure 2 that the GPC curves for the copolymers at various reaction times are quite different from those for its starting PCL diol and PPF precursor with one single broad curve at lower elution volume, which means the copolymer has a higher molecular weight and contains little starting homopolymers. This is in contrast with the extra unconverted PPF's GPC peaks in the synthesis of P(PF-*co*-EG).[4] Figure 3 shows the FTIR spectra for the copolymer samples after polymerizing for 1−4 h with the normalized absorption intensity for the

Table 2. Molecular Weights and Physical Properties of Polymers Herein

	copolymer/PCL		PPF		thermal properties (°C)					
polymer	M_w (g mol^{-1})	M_n (g mol^{-1})	M_w (g mol^{-1})	M_n (g mol^{-1})	T_g (°C)	T_m (°C)	ΔH (J/g)	χ_c (%)	T_d (°C)	density (g cm^{-3})
PCL530	1270	770			−80.6	26.2	67.5	50.0	354	1.073
PCL1250	3030	1710			−73.5	43.4	61.1	45.3	386	1.073
PCL2000	5320	3970			−68.5	48.7	76.7	56.8	392	1.073
PPF1hr			1130	800	−22.4				336	1.239
PPF3hr			2530	1460	2.8				343	1.267
PPF7hr			7910	3460	24.2				351	1.276
copolymer **1**	20800	6010	1300	810	−22.9				350	1.231
copolymer **2**	14300	5220			−21.8				360	1.219
copolymer **3**	21100	6800	1200	750						
copolymer **4**	25200	6180	1210	750	−20.5				346	1.209
copolymer **5**	21200	5590	2710	1410	−16.9				359	1.206
copolymer **6**	8230	4030			−24.0				359	1.202
copolymer **7**	12900	5530	1990	1110	−25.3				359	1.206
copolymer **8**	23200	8610	980	630	−31.9				364	1.198
copolymer **9**	24700	7440	1090	700	−29.6				360	1.191
copolymer **10**	13600	6730	1010	680	−40.1				377	1.169
copolymer **11**	47100	11600	1110	730	−45.9				373	1.180
copolymer **12**	30700	14300	1710	960	−56.0	34.3	38.7	33.0	395	1.117
copolymer **13**	36600	16100	1500	870	−52.8	26.4	38.4	35.1	394	1.124
copolymer **14**	18300	8570	1510	870	−49.2	21.1	0.07	0.07	391	1.122
copolymer **15**	36800	17200	900	620	−53.8	19.7	6.85	6.59	392	1.125
copolymer **16**	28600	14200	1640	950	−57.0	41.8	48.4	39.8	396	1.102

−C═O group at 1730 cm^{-1}, which is constant during the copolymerization. As indicated in Figures 2 and 3, the hydroxyl groups in the polymerizing mixture at 3440 cm^{-1} drop significantly, and the molecular weight increases dramatically in the first hour of copolymerization. After reacting for 4 h, the hydroxyl groups start to be invariant and the molecular weight increases only slightly. DSC curves (not shown in this paper) for those copolymers at different reaction times also support this conclusion by showing the gradually diminishing exothermal peaks for semicrystalline PCL diol.

The molecular weights of all the polymers as well as the starting PPF precursors sampled after step 2 are given in Table 2. Three PCL diols are named after the nominal molecular weights; three PPF samples were synthesized via step 2 for 1, 3, and 7 h for the purpose of comparison. All the copolymers in Table 2 are named after the run numbers in Table 1. In agreement with the earlier studies on P(PF-*co*-EG),[4] the molecular weight of PPF precursors plays an insignificant role in the final copolymer's molecular weight, and the copolymerization time of 5 h is sufficiently long for obtaining high molecular weight without causing thermal crosslinking. The polydispersity of the obtained copolymers ranges from 2.0 to 4.1, which is reasonably larger than that of their homopolymer precursors.

The FTIR spectra of copolymers **8** and **10** as well as those of the starting homopolymers PCL530, PPF1hr, and PPF3hr are presented in Figure 4. The absorption peaks in copolymers' spectra are the combination of those of the two components in them. As marked in Figure 4, carbonyl stretching at 1720 cm^{-1}, C═C stretching at 1645 cm^{-1}, and methylene scissoring and asymmetric bending at 1455 cm^{-1} were all evident in the FTIR spectra of PPF samples and two copolymers. As discussed earlier, hydroxyl absorption is strong at 3440 cm^{-1} for PCL530 and oligomeric PPF1hr while it diminishes for higher molecular weight PPF and copolymers. Methylene absorption at 2940 cm^{-1} can also

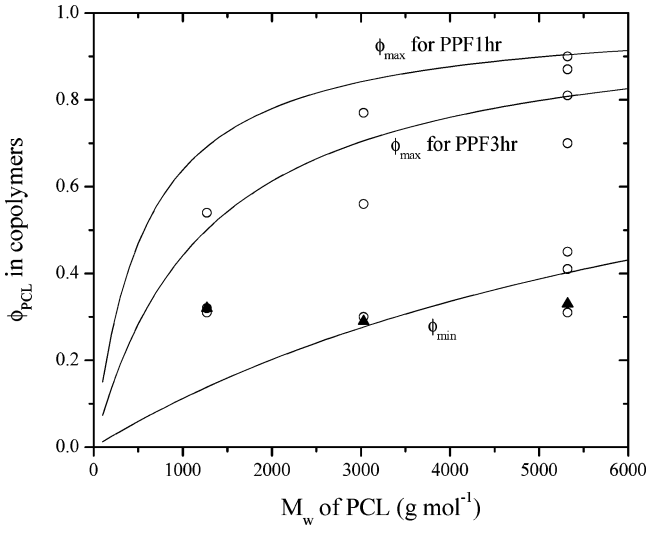

Figure 1. Anticipated maximum and minimum limits (solid curves) for PCL composition (ϕ_{PCL}) in copolymers and PCL feed ratios (symbols) against the PCL diol molecular weight (○, copolymers started from PPF1 h; ▲, copolymers from PPF3hr; the curves for ϕ_{min} and ϕ_{max} for PPF1hr and -3hr are drawn using equations in the text with M_2 = 1130 and 2530 g mol^{-1}, respectively).

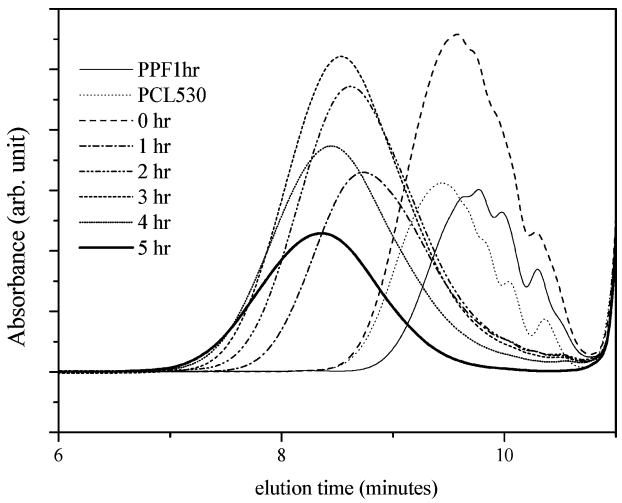

Figure 2. GPC curves of P(PF-*co*-CL) copolymer **10** at the reaction times of 0−5 h as well as PCL530 and PPF1hr.

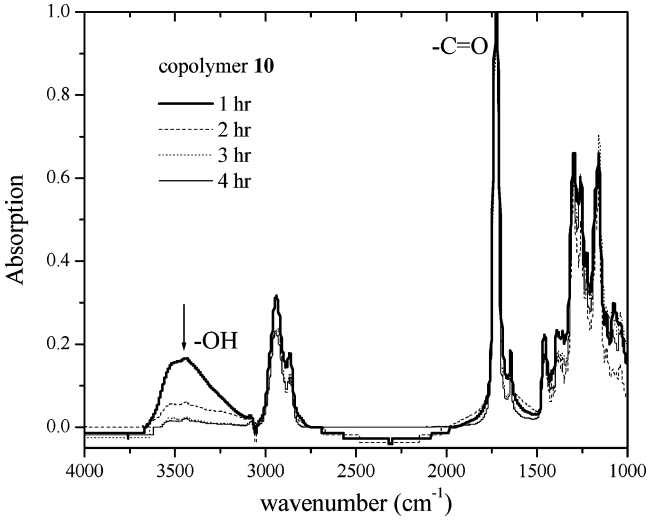

Figure 3. FTIR spectra of P(PF-*co*-CL) copolymer **10** at various reaction times.

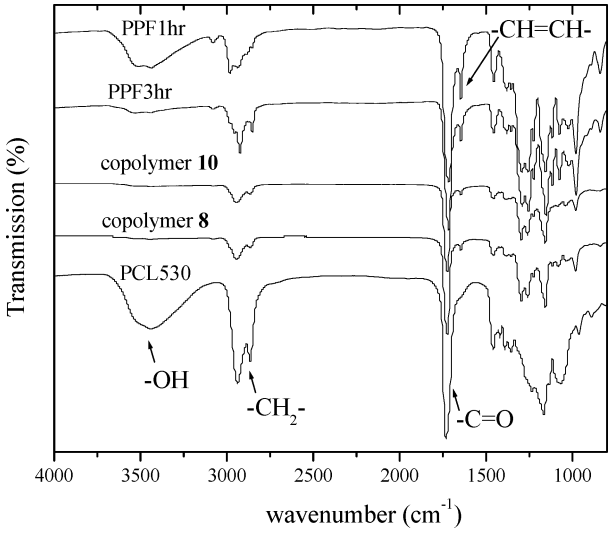

Figure 4. FTIR spectra of oligomeric PPF precursors, PCL530, and P(PF-*co*-CL) copolymers.

be found in all the polymers in Figure 4 with the strongest one in PCL530 due to the highest methylene content in PCL backbone. The peak at 773 cm^{-1} was assigned to the amorphous phase of the copolymers and PPF.

The ^1H NMR (Figure 5) and ^{13}C NMR spectra (Figure 6) of copolymer **1** as well as its parent homopolymers were obtained in deuterated chloroform to determine the chemical structure of the polymers herein. All the chemical shifts can be well assigned to corresponding protons and carbons in the polymer backbone as indicated in Figures 5 and 6. The chemical shifts with peak positions at 1.20−1.40, 4.2−4.4, 5.2−5.4, and 6.8−6.9 ppm shown in the ^1H NMR spectra of both PPF1hr and -7hr can be attributed to methyl, propyl methylene, methylene, and olefinic protons, respectively. There are five additional chemical shifts centered at 1.25, 1.30, 3.72, 4.10, and 5.11 ppm in the ^1H NMR spectrum of PPF1hr. As indicated in the earlier investigations on PPF[3] and poly(1,2-propylene adipate),[15] those chemical shifts are due to different protons (marked as b′, c′, d′ or b″, c″, d″) adjacent to two different types of chain ends based on different acylations of propylene glycol. These chemical shifts disappeared for higher molecular weight PPF or copolymers, which further confirms the

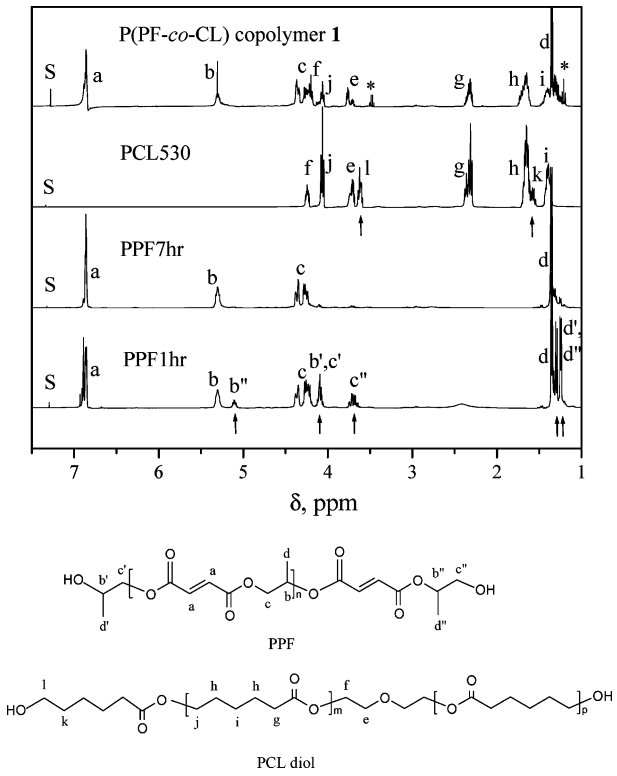

Figure 5. ^1H NMR (400.1 MHz, $CDCl_3$, reference TMS) spectra of P(PF-*co*-CL) copolymer **1**, PCL530, PPF3000, and PPF1hr. S = solvent. Asterisks indicate signals due to diethyl ether, and arrows indicate signals due to protons adjacent to end groups.

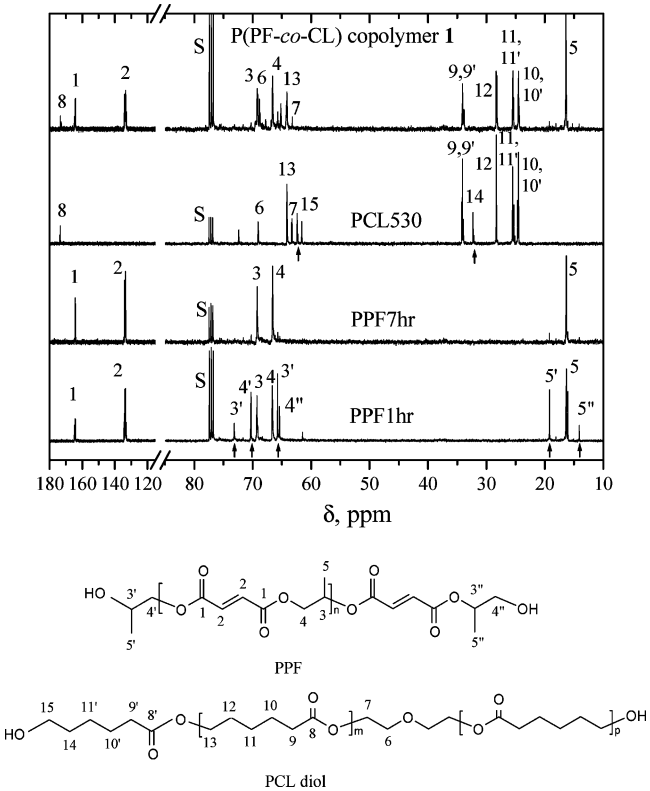

Figure 6. ^{13}C NMR (100.6 MHz, $CDCl_3$, reference TMS) spectra of P(PF-*co*-CL) copolymer **1**, PCL530, PPF3000, and PPF1hr. S = solvent. Arrows indicate signals due to carbons adjacent to end groups.

copolymerization of PPF blocks with PCL diols. In the ^1H NMR spectrum of PCL530, the chemical shifts with

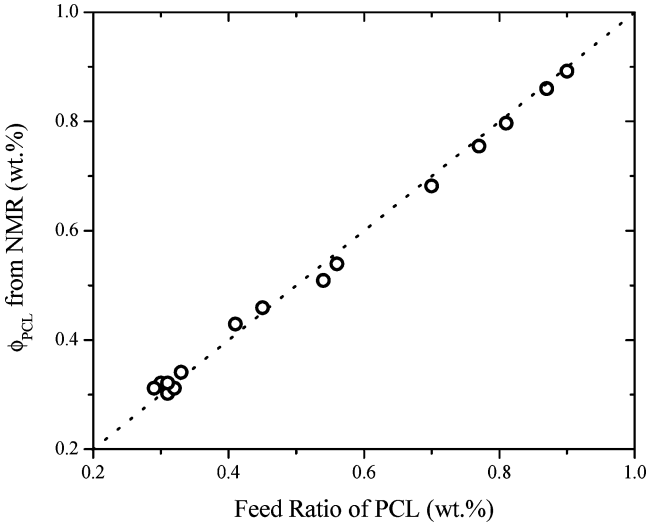

Figure 7. PCL composition in copolymers calculated from ^{1}H NMR integration vs PCL feed ratio.

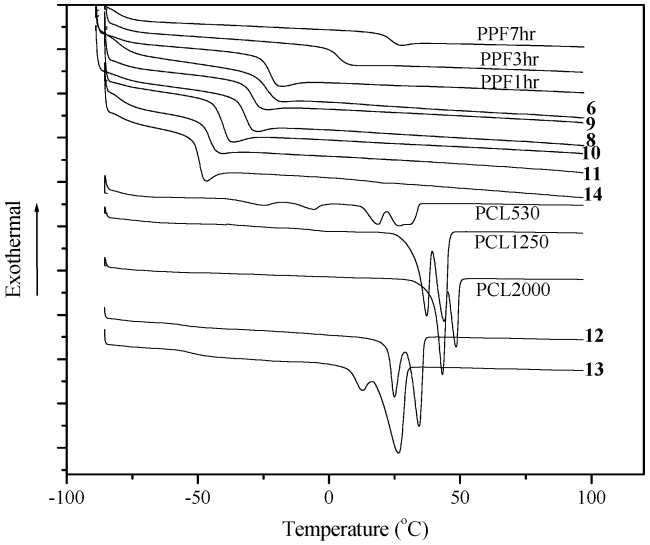

Figure 8. DSC curves of P(PF-*co*-CL) copolymers shown with run numbers and their parent polymers.

peak positions at 1.38, 1.65, 2.31, and 4.06 ppm are assigned to methylene protons of PCL attached to different groups. The chemical shift centered at 3.63 ppm is due to terminal methylene protons of PCL attached to a $-CH_2$ and a hydroxyl end group. There are two additional chemical shifts at 3.71 and 4.24 ppm for all the PCL diols because of the initiator of diethylene glycol used in the ring-opening polymerization of ϵ-caprolactone. The integrations of the chemical shifts at 3.71, 4.24, and 3.63 ppm in the ^{1}H NMR spectra for all the three PCL diols are almost the same, as expected according to the chemical structure. In the ^{13}C NMR spectra of PPF7hr in Figure 6, there are five major chemical shifts at 16.4, 66.6, 69.2, 133.5, and 164.4 ppm. For oligomeric PPF1hr, five chemical shifts due to the carbons adjacent to hydroxyl end groups at 14.1, 19.2, 65.8, 70.3, and 73.2 ppm are much stronger than those of PPF7hr. The chemical shifts in ^{13}C NMR spectrum of PCL530 are at 24.6, 25.5, 28.3, 32.3, 34.1, 61.5−63.3, 64.1, 69.1, 72.5, and 173.6 ppm. Two chemical shifts at 32.3 and 63.4 ppm are due to two carbons (C14 and C15 as marked using arrows in Figure 6) adjacent to the hydroxyl end groups, and two chemical shifts at 63.3 and 69.1 ppm are due to two carbons (C7 and C6) in the segment of diethylene glycol, in agreement with DEPT-135 ^{13}C NMR spectra of P(PF-*co*-EG) and PEG-diacrylate.[4] Both ^{1}H and ^{13}C NMR spectra of copolymer **1** show a good combination of the two components in the copolymer with the disappearance of several chemical shifts related to chain ends in oligomeric PCL530 and PPF1hr.

The integration ratio of peak centered at 6.85 ppm to the one at 2.31 ppm in the ^{1}H NMR spectra of the copolymers can be used to calculate the copolymer compositions. Table 1 and Figure 7 show the results are in good agreement with the feed ratios as thus shown. Because the deviation is within 0.03, the feed ratios for PCL are used as PCL compositions in the later discussions for simplicity without affecting the conclusion.

Thermal Analysis and Morphological Changes. DSC was used to determine melting points (T_m), glass transition temperatures (T_g), and heats of fusion for polymers (ΔH_m). All the thermal properties are listed in Table 2. The glass transition temperatures were determined using the midpoint temperature of the glass transitions. The melting temperatures for the polymers were obtained from the highest temperature of all the exothermal peaks. As indicated in our previous study,[16] T_g increases with the number-average molecular weight expressed as Fox−Flory equation

$$T_g = T_g^{\infty} - \frac{A}{M_n} \quad (1)$$

for PPF with molecular weights studied here, in which A is a constant of 45 100 for PPF and T_g^{∞} is the extrapolated glass transition temperature 31.9 °C for infinite molecular weight. Only when the number-average molecular weight is higher than 5000 g mol^{-1} does T_g start to show molecular weight independence.[16] Such molecular weight dependence also exists for both T_g and T_m in the three PCL diols used in this study.

PCL is a semicrystalline copolymer, and there are crystalline peaks in DSC curves of three PCL diols as shown in Figure 8; however, it is evident that the copolymers are amorphous when the PCL composition is less than 70%. It is quite different from the remaining crystalline structure for another copolymer P(PF-*co*-EG)[4] even when the PEG composition is as low as 47%. The DSC analysis of PCL2000/PPF7hr blends (not shown in this paper) indicates that the copolymerization of semicrystalline PCL with amorphous PPF indeed suppressed the crystallinity more efficiently than blending those two components. The amorphous morphology here is reminiscent of the amorphous copolymer of glycolic acid and lactic acid, which has a much higher degradation rate than its parent polymers: highly crystalline poly(glycolic acid) (PGA) and hydrophobic poly(lactic acid) (PLA).[17] There is only a single glass transition for all the copolymers, suggesting the absence of microphase separation in amorphous phase. Moreover, the glass transitions for all the copolymers are as narrow (about 10 °C) as that for PPF and confirm that the copolymerization was quite successful since the single glass transition for miscible polymer blends is generally much broader than those pure polymers due to microheterogeneity resulting from different local chain friction coefficients for different components.[18] It should be noted in Figure 8 that T_g for the copolymer decreases while T_m increases with increasing PCL composition. The crystallinity χ_c of PCL in the copoly-

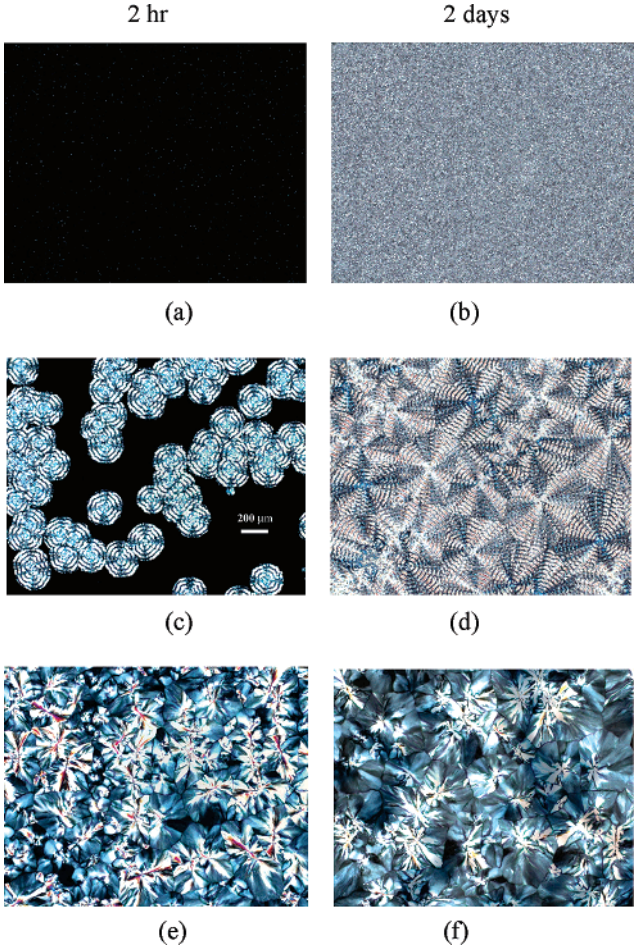

Figure 9. Polarized optical microscopic graphs of (a) copolymer **13** with PCL content of 80%, (c) copolymer **12** with PCL composition of 87%, (e) pure PCL2000 for 2 h crystallization at room temperature; graphs in (b), (d), and (f) correspond to samples in (a), (c), and (e) after 2 day crystallization at room temperature (magnification: 200×; the scale bar of 200 μm in (c) is applicable for all the graphs here).

mers can be calculated from the ΔH_m values of copolymers, completely crystalline PCL (ΔH_m^c = 135 J/g),[19] and the PCL composition ϕ using the equation of $\chi_c = [\Delta H_m/(\phi \Delta H_m^c)] \times 100\%$. The crystallinity of the three PCL diols is around 50%, and it drops significantly to around 30% when amorphous PPF segments were introduced to the copolymer backbone. Eventually, the crystallinity diminishes when the PCL composition is lower than 70%. Similar to the trend in P(PF-*co*-EG),[4] the melting point drops from 48.7 °C to 34.3, 26.4, 21.1 °C, and the melting peaks become broader correspondingly for a fixed PCL block with M_n of 3970 g mol^{-1}, indicating that smaller and less uniform crystallites were formed.

To support the thermal analysis using DSC, polarized optical microscopic (POM) graphs of three polymers with different PCL compositions are shown in Figure 9. Copolymers **12**, **13**, and PCL2000 were first melt at 100 °C and then quenched to room temperature. The POM pictures were taken after crystallizing at room temperature for 2 h (a, c, e in Figure 9) and 2 days (b, d, f in Figure 9). As expected, well-developed spherulites can be observed for PCL2000. More interesting to note is that concentric bands with a defined Maltese cross extinction pattern were observed in the spherulites of copolymer **12** with a high PCL composition of 87%, while the spherulites grown at room temperature in pure PCL2000 and other copolymers such as copolymer **13** in Figure 9 had no ring patterns. The spacing for these ring patterns in Figure 9c,d is commonly in the vicinity of 25 μm. Such spacing is supposed to change with the crystallization temperature and amorphous component composition in the copolymers or blends according to the investigations on the other polymer systems.[20−24] For the copolymers with PCL compositions less than 70%, both DSC curves and POM graphs show no crystallinity at all, in contrast to a fairly high crystallinity for PCL2000/PPF7hr blend at the same PCL composition. As shown in Figure 9a,b, the growth rate of the imperfect PCL crystalline structure is greatly impeded by the amorphous however rigid PPF segments in the copolymers. The crystalline structure indicated in the DSC curve can be seen under POM (Figure 9b) only after 2 day crystallization.

The presence of banded spherulites is well-known for polyethylene,[20] poly(3-hydroxybutyrate) (PHB),[21] and miscible blends of PCL with styrene−acrylonitrile copolymer (SAN),[22] poly(vinyl chloride) (PVC),[23] or other polymers.[24] It was also reported that PCL banded spherulites could be achieved at a high crystallization temperature such as 50 °C.[22−24] Such banded spherulite could also be found in the diblock or triblock copolymers consisting of PCL segments such as polybutadiene-*co*-polycaprolactone (BC) and polystyrene-*co*-polybutadiene-*co*-polycaprolactone (SBC) at certain PCL compositions.[10] It should be pointed out that copolymer **12** is supposed to be triblock-like as PCL-*co*-PPF-*co*-PCL at such a high PCL composition. To our knowledge, it is the first time to report such a banded pattern in PCL spherulite in triblock copolymers with PCL end-blocks. It is well accepted that the periodic extinction of banded spherulites is due to the lamellar twisting along the radical direction during crystal growth although the mechanisms are not yet well understood.[10,20−24] The extensive studies by Keith and Padden[28] showed the axial rotation of the lamellae is caused by surface stresses. The more pronounced surface stress of the PCL lamellae in the block copolymer compared to that in PCL miscible blends, together with the impeded crystal growth rate, might be the major origin of this banded pattern. Further detailed studies on such banded spherulite in PCL copolymers are being performed by the authors.

Thermogravimetric analysis (TGA) has been performed to determine the weight loss when the temperature increases. As depicted in Figure 10 for a typical copolymer (**6**) and its parent homopolymers, there is only one degradation step for all the polymers and the thermal stability of the copolymer is between those of its parent polymers PCL and PPF. The onset degradation temperatures (T_d) of all the polymers herein are listed in Table 2, and it increases with the semicrystalline PCL composition in the copolymers from 336 °C for PPF1 h to 392 °C for PCL2000. Similar to other two characteristic temperatures T_g and T_m determined by DSC, T_d also has molecular weight dependence in the molecular weight range for all these oligomeric PCL and PPF samples. However, the influence of molecular weight on the copolymers' physical properties here is not significant because of fairly larger molecular weights compared to their parent polymers. The more dominant factor here is the copolymer composition.

The phase diagram in Figure 11 summarizes the characteristic temperatures (T_g, T_d, and T_m) for the 15

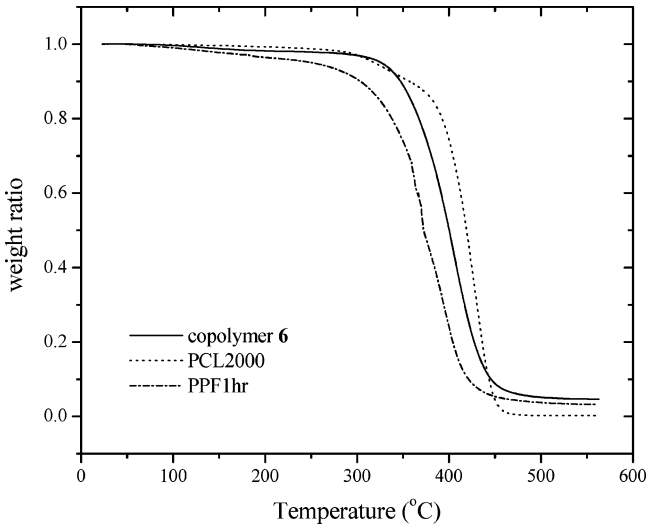

Figure 10. TGA thermograms of oligomeric PPF1hr, PCL2000, and P(PF-*co*-CL) copolymer **6**.

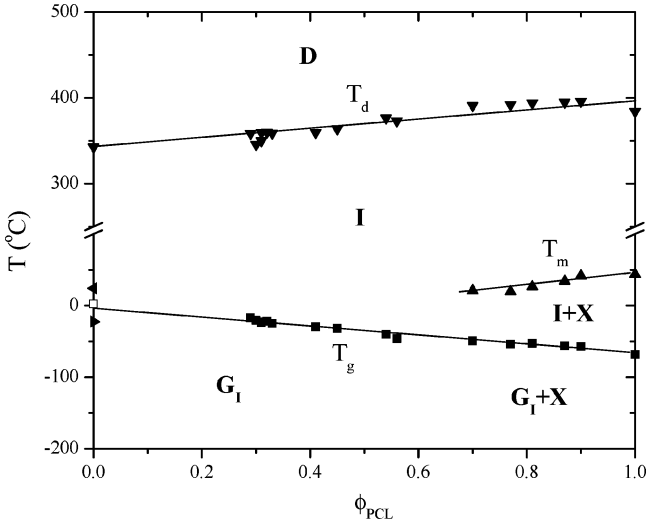

Figure 11. Phase diagram of P(PF-*co*-CL) vs PCL composition: D, degradation; I, isotropic liquid; G_I, isotropic glass; and X, crystalline phase. T_g (■), T_m (▲), and T_d (▼): glass transition, melting, and degradation temperatures. The lines were drawn by the naked eye. The glass transition temperatures for PPF1hr, -3hr, and -7hr are shown as symbols ▲ (pointing right), □, and ▲ (pointing left), respectively, on the *y*-axis at $\phi_{PCL} = 0$.

copolymers and their parent polymers as a function of PCL composition. As mentioned earlier, no melting point and no crystalline behavior could be observed for PCL composition less than 70%. Besides the composition effect, T_g and T_m become closer at lower PCL composition, and the glass domains lead to "nanoscale confinement" of PCL lamellae, preventing the subsequent crystallization of the PCL block. The line formed by the glass transition temperatures delineates the boundary between isotropic glass (G_I) and isotropic liquid (I) phases. When the PCL composition exceeds 70%, crystalline structure starts to show up and one additional crystalline phase (X) exists in the phase diagram before the copolymers enter the isotropic phase when the temperature is above T_m. As revealed in the earlier studies on PCL block copolymers, the crystallinity of PCL block will be significantly influenced by the PCL block length.[10] Therefore, the crystallinity might be quite different at the same PCL composition although the melting point for copolymer **15** with PCL1250 blocks

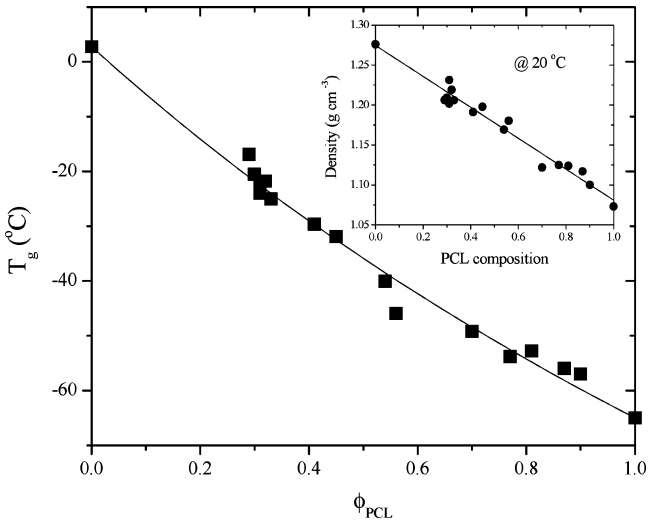

Figure 12. Glass transition temperatures vs PCL composition in the copolymers. The prediction of the Fox equation is also shown as the curve. Inset: polymer density at 20 °C vs PCL composition.

falls on the line formed by T_m of the copolymers with PCL2000 blocks. Polymers start to degrade thermally when the temperature is beyond the line formed by T_d. A similar phase diagram can be found for another copolymer based on PPF, P(MPF-*co*-PF),[6] in which a nematic mesophase with schlieren textures was found after introducing rigid block with methylphenylene rings. In Figure 11, the composition dependence for T_g is depicted as a straight line for simplicity. When we enlarge the part for T_gs in Figure 12, the curvature dependence can be satisfactorily predicted by the Fox equation

$$\frac{1}{T_g} = \frac{\phi_{PCL}}{T_{g,PCL}} + \frac{\phi_{PPF}}{T_{g,PPF}} \qquad (2)$$

as the curve through the experimental points when $T_{g,PCL}$ and $T_{g,PPF}$ are set to −65 and 2.75 °C, respectively. As also revealed in Figure 11, the T_g values here in the Fox equation for PCL and PPF are between those for infinite long chains (−60 and 31.9 °C, respectively) and those for their oligomeric counterparts (e.g., PPF1hr and PCL530) originated from the effects of both chain environment and chain length. Meanwhile, the density information for all the polymers is also given in Table 2 and the inset of Figure 12, ranging from 1.073 for PCL diols to 1.276 for PPF with a good linearity of composition dependence.

Rheological Measurements. Rheological measurements have been performed on copolymers and their parent homopolymers at various temperatures to obtain zero-shear viscosity η_0 as well as storage and loss moduli G' and G''. The data of η_0 at 40 °C are tabulated in Table 3. The time−temperature superposition (tTs) was applicable for all the polymers here in the temperature range studied, and the master curves reduced to a reference temperature of 25 °C were formed as shown in Figure 13. Although no direct measurement was done for PPF7hr at 25 °C, for comparison the master curve for PPF7hr was shifted to 25 °C based on the information at other temperatures. It can be seen from the master curves that almost all the copolymers and PPF7hr here are unentangled as G' and G'' do not have a crossover point to indicate the entanglement. In the

Table 3. Results of Melt Rheology and Dilute Solution Viscometry for Copolymers

polymer	η_0 (Pa s) at 40 °C	C_1[a]	C_2 (°C)[a]	[η] (dL g^{-1})[b]	k_{H1}[c]	k_{H2}[c]
copolymer **1**	990	6.28	119.6	0.102	0.47	0.37
copolymer **2**	530	5.46	105.4	0.081	1.11	
copolymer **4**	1940	6.33	96.0	0.107	0.36	0.43
copolymer **5**	1740	5.66	89.7	0.097	0.90	
copolymer **6**	210	3.46	65.4	0.079	0.96	
copolymer **7**	480	4.03	70.5	0.104	0.42	0.31
copolymer **8**	840	5.82	126.7	0.142	0.50	
copolymer **9**	710	4.90	99.6	0.132	0.52	
copolymer **10**	91	3.92	116.1	0.119	0.37	
copolymer **11**	210	4.12	118.1	0.168	0.51	
copolymer **12**				0.289	0.37	
copolymer **13**	400	4.36	148.0	0.293	0.48	
copolymer **14**	86	4.30	144.7	0.148	0.49	
copolymer **15**	390	3.37	110.8	0.415	0.47	
copolymer **16**				0.264	0.46	

[a] Obtained from the horizontal shift factors a_T at the reference temperature $T_0 = 25$ °C for all the samples. [b] Intrinsic viscosity was measured in toluene at 30.0 ± 0.05 °C. [c] The quadratic term was analyzed to get k_{H2} for curves with curvature; otherwise, only k_{H1} was given from the slope in Figure 16.

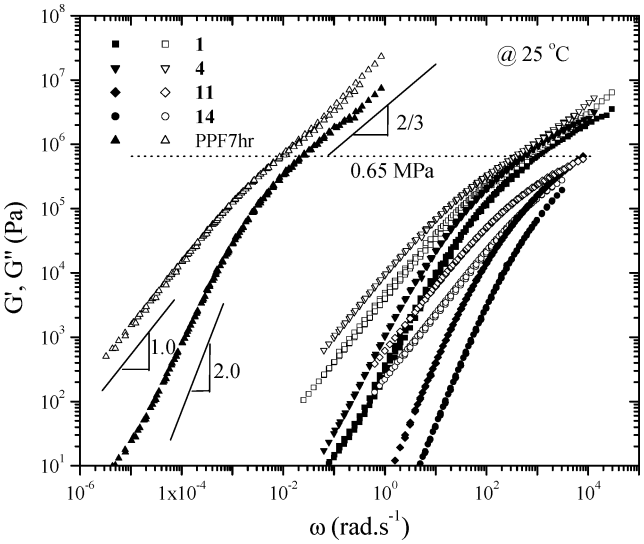

Figure 13. Master curves of G' and G'' for PPF7hr and copolymers at the reference temperature of 25 °C. Solid symbols, G'; open symbols, G''.

terminal regime at low frequencies, all the polymers show typical relations in G' and G'' functions as $G' \propto \omega^2$ and $G \propto \omega^1$. Since there is no plateau regime for G' and G'', the curves directly go to glass regime (G', $G \propto \omega^{2/3}$) at higher frequencies from the terminal regime.[26] The transition region is rather broad compared to the monodisperse polymer due to a broader distribution of relaxation spectrum. Similar to many other polymers, a stronger exponent 2/3 was found in the frequency dependence of G' and G'', showing departure from the estimate G', $G \propto \omega^{1/2}$ based on the Rouse model.[26] The crossover frequency for entangled polymer systems can be used as the reciprocal of the longest relaxation time.[27] For unentangled systems here, the relaxation times can be estimated by using the position of G' and G'' master curves.[27] It is apparent in Figure 13 that the relaxation times decrease dramatically as much as 4−5 decades through changing chain friction coefficient and flexibility after introducing PCL segments into PPF backbone, despite the copolymer molecular weight is higher than that of PPF7hr. A plateau modulus G_N^0 of 0.65 MPa can be roughly estimated for all the polymer species in Figure 13 from the transition from the terminal regime to glassy regime.

The zero-shear viscosities, η_0, were obtained in the terminal region when the viscosity shows Newtonian behavior with frequency and can be expressed as[26]

$$\lim_{\omega \to 0} \frac{G'(\omega)}{\omega} = \eta_0 \tag{3}$$

The measured η_0 at 40 °C for all the polymers are shown in Table 3, and the temperature dependence of η_0 for all the copolymers and two homopolymers (PPF3hr and PCL2000) is shown in Figure 14a. It can be seen in Figure 14a that the temperature dependence for η_0 varies with PCL composition. A smooth progression with increasing PCL composition in the copolymers is evident in the inset of Figure 14a when viscosity data were normalized to the value at 40 °C. The temperature dependence for PPF3hr is the strongest, and the viscosity ranges over as much as 6 orders of magnitude when the temperature changes from 10 to 100 °C, while it is rather weak for PCL2000 and other copolymers with high PCL compositions. Usually the temperature of the melt viscosity is modeled with three different mechanisms, which involve Arrhenius equation for $T > T_g + 100$ °C

$$\eta(T) = K_a \exp\left(\frac{E_a}{RT}\right) \tag{4}$$

The Williams−Landel−Ferry (WLF) equation[26] for $T_g + 20$ °C $< T < T_g + 100$ °C

$$\log a_T = \log\left[\frac{\eta(T)}{b_T \eta(T_0)}\right] = -\frac{C_1(T - T_0)}{C_2 + (T - T_0)} \tag{5}$$

and fragility

$$m = \left.\frac{\partial \log \eta(T)}{\partial (T_g/T)}\right|_{T=T_g} \tag{6}$$

for temperatures close to T_g, respectively. In these equations above, K_a is a constant, R is the universal gas constant, E_a is the activation energy, and a_T and b_T are the horizontal and vertical shift factors in tTs, respectively. Since b_T depends very weakly on temperature, it is close to unity and can be ignored safely here. Therefore, a_T stands for the ratio of the viscosity at the temperature of T to that at the reference temperature T_0. C_1 (dimensionless) and C_2 (in °C) are two constants.

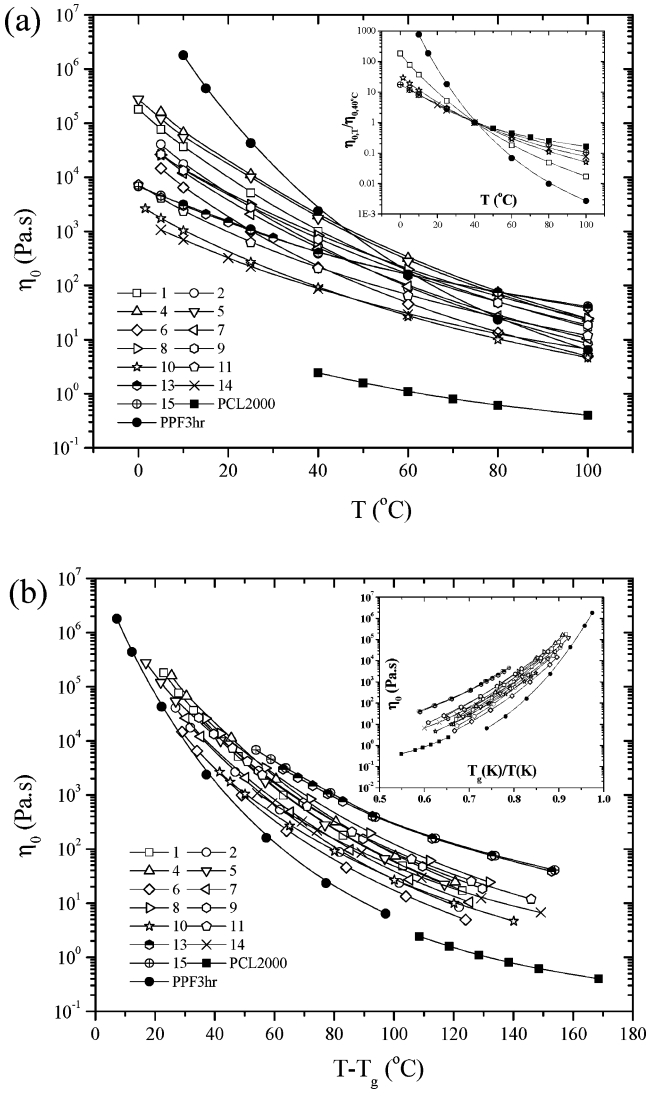

Figure 14. Viscosities vs (a) T, (b) $T - T_g$, and inset of (b) T_g/T for PPF3hr, PCL2000, and copolymers with run numbers in the legend. Inset in (a): normalized viscosity to the temperature of 40 °C vs temperature for PPF3hr, copolymers **1**, **10**, **14**, **15**, and PCL2000.

The temperature dependence for viscosity here can be expressed using the WLF equation with C_1 and C_2 shown in Table 3 when the reference temperature is 25 °C.

The temperature dependences of η_0 in Figure 14a can be replotted against $T - T_g$ or T_g/T in Figure 14b to reach the isofriction state approximately. In contrast with earlier investigations on PPF,[16] poly(dimethylsiloxane) (PDMS)[28] with different molecular weights, and (styrene-*b*-isoprene-*b*-styrene-*b*-isoprene) tetrablock copolymers[29] with various compositions, the changing temperature dependence of η_0 with the PCL composition still exists in Figure 14b. Limited by the temperature window of rheological measurements, the melt viscosities at temperatures close to T_g are not reachable. Nevertheless, determined by the chemical structure of PPF, higher fragility for copolymers with higher PPF composition is implied from the inset of Figure 14b and eq 6. It was also revealed in polystyrene[30] that molecular weight also has significant influence on polymer fragility when the molecular weight is smaller than a critical one; however, it is not within the scope of the present paper.

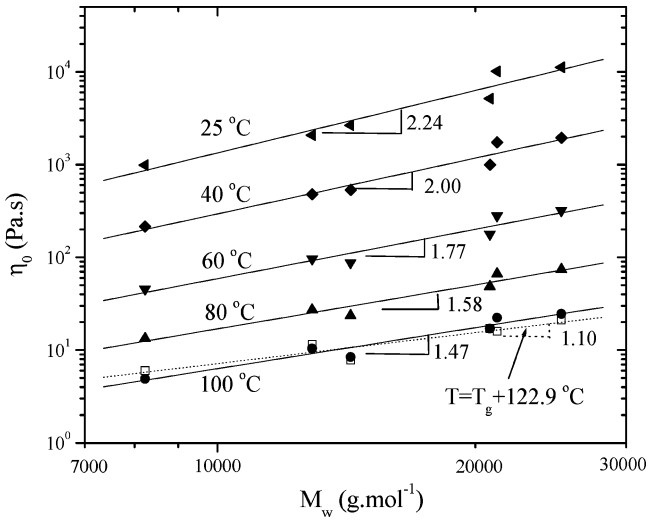

Figure 15. Molecular weight dependence of zero-shear viscosity at six different temperatures for copolymers **1**, **2**, and **4**−**7** with a PCL composition of around 30 wt %.

For unentangled and entangled polymers, it is well-known that the molecular weight dependence for melt viscosity can be described as $\eta_0 \propto M^{1.0}$ using the Rouse model and $\eta_0 \propto M^{3.0}$ using the reptation model.[26,27,31,32] Since both Rouse model and reptation model are single-chain approaches, they have been modified to interpret the stronger molecular weight dependences in polymer melts. Specifically, isofriction correction using chain-end free volume theory is for unentangled systems while contour length fluctuations and constraint release for entangled systems.[26,27,31,32] In addition, the role of chain statistics in unentangled systems has attracted much attention recently.[33] However, the origins and roles of these corrections in important parameters such as viscosity, relaxation time, plateau modulus, and diffusion coefficient are still in debate.[27b,c] Figure 15 shows the molecular weight dependence of the viscosity for six copolymers (**1**, **2**, **4**−**7**) with a similar PCL composition of ∼30% at various temperatures. The linearity in Figure 15 suggests the microstructure such as block length and distribution does not influence the macroscopical property η_0 strongly, as long as the block composition is fixed. Therefore, such copolymers are like polybutadiene consisting of both 1,4- and 1,2-microstructures, in which T_g increases with 1,2-content systematically.[34] The exponent a in $\eta_0 = kM^a$ decreases from 2.24 at 25 °C to 1.47 at 100 °C, indicating the unentangled characteristics of these six samples and the weakened free volume effect at higher temperatures. The Rouse prediction $\eta_0 \propto M^{1.0}$ can be satisfactorily approached ($\eta_0 \propto M^{1.10}$) after isofriction correction by measuring the viscosity at the temperature with the same distance ($T - T_g = 122.9$ °C) from the copolymers' T_g.

Solubility and Dilute Solution Properties. Similar to their parent polymers PPF and PCL, all the copolymers are hydrophobic. They are insoluble in water, methanol, hexane, and diethyl ether; while they can be dissolved easily in methylene chloride, tetrahydrofuran, acetone, dimethylformamide, and toluene at ambient temperature. It should be noted that the solubility of the copolymers in toluene is greatly enhanced by introducing PCL segments to the copolymers considering toluene is a poor solvent for PPF at room temperature. Another copolymer P(PF-*co*-EG)[4] is highly amphiphilic due to the different solubility of two seg-

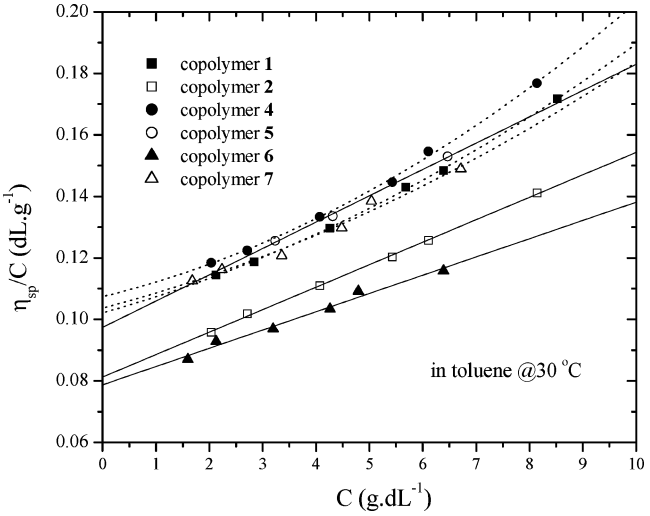

Figure 16. η_{sp}/C vs concentration C for copolymers **1**, **2**, and **4**−**7** in toluene at 30 °C (solid lines, linear fits; dotted curves, second-order fits).

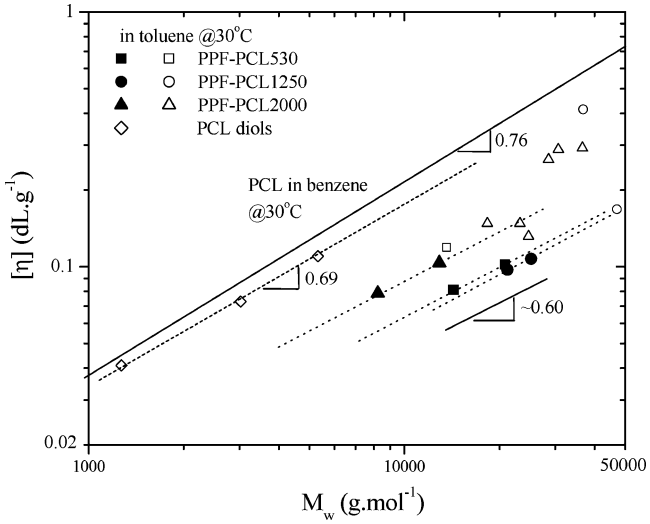

Figure 17. Molecular weight dependence of intrinsic viscosity [η] for copolymers at 30 °C in toluene as well as three PCL diols. The copolymer pairs **1**−**2**, **4**−**5**, and **6**−**7** with a PCL composition of around 30% are shown as solid symbols with a dotted line through them; the rest of the copolymers are shown as open symbols. The solid line is for PCL in benzene at 30 °C in ref 36.

ments PPF and PEG. The solubility and assembly morphology of the copolymers in solutions can be modulated through varying the content, length, and the arrangement of different blocks with hydrophilic or hydrophobic properties.

The intrinsic viscosity [η] of the copolymers and PCL samples in toluene at 30 °C was measured using the Huggins equation[26]

$$\eta_{sp}/C = [\eta]\{1 + k_{H1}[\eta]C + k_{H2}[\eta]^2C^2 + ...\} \quad (7)$$

where η_{sp} is specific viscosity, C is concentration in g dL^{-1}, and k_{H1} and k_{H2} are the first- and second-order concentration coefficients. When the concentration is low enough, there is only a linear relationship between η_{sp}/C and C, and k_{H1} is also known as Huggins coefficient. Since some experimental data sets exhibit curvature as shown in Figure 16, the second fitting was applied to get concentration coefficients and [η] from the intercepts at concentration zero. The results of dilute solution viscometry are listed in Table 3. For copolymers (**1**, **2**, **4**−**7**) with low PCL compositions, k_{H1} values from first-order fit are as large as close to unity although second-order fit gives smaller k_{H1} values for copolymers **1**, **4**, and **7**. It implies that toluene at 30 °C is nearly a θ-solvent for copolymers **1**, **2**, and **4**−**7**. When PCL composition in the copolymers increases further, k_{H1} values range from 0.37 to 0.52, indicating a more flexible chain in a relative good solvent.

Although the molecular weight dependence of melt viscosity for copolymers **1**, **2**, and **4**−**7** in Figure 15 does not show much microstructure influence, the microstructure indeed plays an important role in intrinsic viscosity's molecular weight dependence as depicted in Figure 17. The intrinsic viscosities for copolymers **1**, **2**, and **4**−**7** are rather scattered when plotted against molecular weight, and the overall slope for the exponent α in Mark−Houwink−Sakurada (MHS) equation [η] = KM^{α} is too small (~0.24) to be reasonable for such linear polymer chains in a solvent. It is apparent that for each pair (**1**−**2**, **4**−**5**, and **6**−**7**) with the same PCL block can give α values of around 0.6. It should be mentioned that only two [η] values were used to construct the linear fit, and those two values in each pair were obtained from different approaches indicated in Figure 16. Linear extrapolation gives lower [η] and higher k_{H1} compared to second-order fitting.[35] Nevertheless, slopes of ~0.6 reasonably support the earlier conclusion that toluene is close to a θ-solvent for copolymers **1**, **2**, and **4**−**7**. The decreasing K values from pair **6**−**7** to **1**−**2** and then **4**−**5** indicate the decreasing chain flexibility, which parallels the increasing T_g in Table 2. Figure 17 also shows some intrinsic viscosities for the other copolymers with higher PCL compositions as well as three PCL diols at the same condition. The MHS equation (dashed line in Figure 17) for three PCL diols is [η] = $3.01 \times 10^{-4}M_w^{0.69}$. The literature MHS equation ([η] = $1.96 \times 10^{-4}M_w^{0.76}$)[36] for PCL in benzene at 30 °C is also shown as a solid line for comparison. It can be observed that the intrinsic viscosities for copolymers with PCL compositions higher than 70% clearly deviate up to the line for PCL from the linear molecular weight dependence (dotted lines in Figure 17) for low PCL composition ones.

Cross-Linking. The detailed information about biodegradation and cross-linking process including the mechanical properties of cross-linked products will be given in a subsequent paper. Here we briefly report the self-cross-linkability and photo-cross-linkability of the copolymers synthesized in the present study. In the thermal-cross-linking process, benzoyl peroxide (BPO) and *N*-dimethyltoluidine (DMT) were used as the free radical initiator and accelerator, respectively. 100 μL of initiator solution (50 mg of BPO in 250 μL of NVP) and 40 μL of accelerator solution (20 μL of DMT in 980 μL of methylene chloride) were added in 1.5 g of P(PF-*co*-CL) solution in 500 μL of methylene chloride and mixed thoroughly. The polymerizing scaffold was transferred into various Teflon molds, and the molds were placed in a convection oven overnight to facilitate cross-linking. All the copolymers can be self-cross-linked without further adding cross-linker because of the enhanced chain flexibility after introducing PCL blocks in the backbone. After cross-linking, the cross-linked polymer was removed from the mold after it was cooled to ambient temperature. A similar cross-linking process can be done to the mixture of copolymers and porogen (salt with various size distributions) to make scaffolds

with different porosity, which can be controlled by the content of porogen. After cross-linking, salt was leached out by placing the scaffolds in distilled water for 3 days. The scaffolds were dried in a vacuum for at least 12 h.

Photo-cross-linking was initiated with ultraviolet (UV) (λ = 315−380 nm) using a photoinitiator bis-(acylphosphine oxide) (BAPO, Ciba Geigy). About 15 mg of BAPO was added into 1.5 g of P(PF-*co*-CL) solution in 500 μL of methylene chloride and mixed thoroughly. The mixture was poured in a mold formed by two glass plates and a Teflon spacer of 1 mm thickness, and the mold was placed directly under UV light for 30 min to facilitate cross-linking. Therefore, such self- and photo-cross-linkable copolymers are promising to construct tissue-engineering scaffolds using a variety of fabrication methods such as stereolithography.

For P(PF-*co*-CL) copolymers with high PCL compositions, the crystallinity-related morphology change around T_m and chemical cross-linking with saturated PCL blocks may render shape-memory effect and swelling properties in organic solvents. These possible interesting properties attract the authors to investigate further on this series of copolymers and explore their use in bone, cartilage, and nerve tube regenerations, equipped with the extensive knowledge of physical properties in this report.

Conclusions

The terminal hydroxyl groups of poly(ϵ-caprolactone) were reacted successfully with poly(propylene fumarate) in a transesterification reaction to form an ester linkage between the two homopolymers. Sixteen different copolymer formulations were investigated, and the molecular structure and molecular weights were determined using various methods to verify the copolymerization. The physical properties such as glass transition temperature T_g, melting temperature T_m, degradation temperature T_d, and polymer density ρ were obtained and indicated strong composition dependences. When the PCL composition is below 70%, the copolymers become amorphous. A banded pattern was observed in the PCL spherulites when the PCL composition in the copolymer is 87% due to the lamellar twisting along the radical direction during crystal growth induced by the strong surface stress and impeded crystal growth rate. Although the copolymer molecular weights are higher than that of PPF, the relaxation of copolymers is much faster and T_g is much lower than that of PPF. The solubility tests showed hydrophobic characteristics of all the copolymers while the solubility in toluene at room temperature was enhanced by the introduction of PCL segments in the copolymers. Dilute solution viscometry also confirms the copolymer chain flexibility is much higher than that PPF. Because of such enhanced flexibility in copolymers after the introduction of PCL blocks, all the copolymers were found to be self-cross-linkable without further adding any cross-linkers and photo-cross-linkable under UV light by adding photoinitiators. Therefore, such copolymers with controllable physical and cross-linking properties can be used as tissue engineering materials in bone, cartilage, and nerve regenerations. The extensive studies on the physical properties supply a platform for investigations on biodegradable multiblock copolymers and reveal an efficient modulation method of polymer properties through making copolymers with various compositions.

Acknowledgment. This work was funded by the Mayo Foundation and National Institutes of Health (R01 AR45871 and R01 EB003060).

Supporting Information Available: Table of the melt viscosities of all the polymers studied here at various temperatures ranging from 0 to 100 °C. This material is available free of charge via the Internet at http://pubs.acs.org.

References and Notes

(1) Temenoff, J. S.; Mikos, A. G. *Biomaterials* **2000**, *21*, 2405.
(2) Gunatillake, P. A.; Adhikari, R. *Eur. Cell. Mater.* **2003**, *5*, 1.
(3) (a) Peter, S. J.; Miller, M. J.; Yaszemski, M. J.; Mikos, A. G. In *Handbook of Biodegradable Polymers*; Domb, A. J., Kost, J., Wiseman, D., Eds.; Harwood Academic Publishers: Amsterdam, 1997; pp 87−97. (b) Yaszemski, M. J.; Payne, R. G.; Hayes, W. C.; Langer, R. S.; Aufdemorte, T. B.; Mikos, A. G. *Tissue Eng.* **1995**, *1*, 41. (c) Yaszemski, M. J.; Payne, R. G.; Hayes, W. C.; Langer, R. S.; Mikos, A. G. *Biomaterials* **1996**, *17*, 2127. (d) Domb, A. J.; Manor, N.; Elmalak, O. *Biomaterials* **1996**, *17*, 411. (e) He, S.; Yaszemski, M. J.; Yasko, A. W.; Engel, P. S.; Mikos, A. G. *Polymer* **2001**, *42*, 1251. (f) Fisher, J. P.; Holland, T. A.; Dean, D.; Engel, P. S.; Mikos, A. G. *J. Biomater. Sci., Polym. Ed.* **2001**, *12*, 673. (g) Peter, S. J.; Miller, M. J.; Yasko, A. W.; Yaszemski, M. J.; Mikos, A. G. *J. Biomed. Mater. Res. (Appl. Biomater.)* **1998**, *43*, 422. (h) Peter, S. J.; Suggs, L. J.; Yaszemski, M. J.; Engel, P. S.; Mikos, A. G. *J. Biomater. Sci., Polym. Ed.* **1999**, *10*, 363. (i) Shung, A. K.; Timmer, M. D.; Jo, S.; Engel, P. S.; Mikos, A. G. *J. Biomater. Sci., Polym. Ed.* **2002**, *13*, 95. (j) Kharas, G. B.; Kamenetsky, M.; Simantirakis, J.; Beinlich, K. C.; Rizzo, A.-M. T.; Caywood, G. A.; Watson, K. *J. Appl. Polym. Sci.* **1997**, *66*, 1123.
(4) Suggs, L. J.; Payne, R. G.; Yaszemski, M. J.; Alemany, L. B.; Mikos, A. G. *Macromolecules* **1997**, *30*, 4318.
(5) Najafi, F.; Sarbolouki, M. N. *J. Appl. Polym. Sci.* **2004**, *92*, 295.
(6) Galcera, T.; Fradet, A.; Marechal, E. *Eur. Polym. J.* **1995**, *31*, 733.
(7) Elfick, A. P. D. *Biomaterials* **2002**, *23*, 4463.
(8) Ng, K. W.; Hutmacher, D. W.; Schantz, J.-T.; Ng, C. S.; Too, H.-P.; Lim, T. C.; Phan, T. T.; Teoh, S. H. *Tissue Eng.* **2001**, *7*, 441.
(9) (a) Wu, Q.; Yoshino, T.; Sakabe, H.; Zhang, H.; Isobe, S. *Polymer* **2003**, *44*, 3909. (b) Lang, M.; Wong, R. P.; Chu, C.-C. *J. Polym. Sci., Polym. Chem.* **2002**, *40*, 1127. (c) Saad, B.; Keiser, O. M.; Welti, M.; Uhlschmid, G. K.; Neuenschwander, P.; Suter, U. W. *J. Mater. Sci., Mater. Med.* **1997**, *8*, 497. (d) Nagata, M.; Kanechika, M.; Sakai, W.; Tsutsumi, N. *J. Polym. Sci., Polym. Chem.* **2002**, *40*, 4523. (e) Turunen, M. P. K.; Korhonen, H.; Tuominen, J.; Seppala, J. V. *Polym. Int.* **2001**, *51*, 92. (f) Kweon, H. Y.; Yoo, M. K.; Park, I. K.; Kim, T. H.; Lee, H. C.; Lee, H. S.; Oh, J. S.; Akaike, T.; Cho, C. S. *Biomaterials* **2003**, *24*, 801. (g) Lim, K. Y.; Kim, B. C.; Yoon, K. J. *J. Polym. Sci., Part B: Polym. Phys.* **2002**, *40*, 2552. (f) Bogdanov, B.; Toncheva, V.; Schacht, E.; Finelli, L.; Sarti, B.; Scandola, M. *Polymer* **1999**, *40*, 3171.
(10) (a) Nojima, S.; Yamamoto, S.; Ashida, T. *Polym. J.* **1995**, *27*, 673. (b) Lovinger, A. J.; Han, B. J.; Padden, F. J., Jr.; Mirau, P. A. *J. Polym. Sci., Part B: Polym. Phys.* **1993**, *31*, 115. (c) Petrova, Ts.; Manolova, N.; Rashkov, I.; Li, S.; Vert, M. *Polym. Int.* **1998**, *45*, 419. (d) Balsamo, V.; von Gyldenfeldt, F.; Stadler, R. *Macromol. Chem. Phys.* **1996**, *197*, 3317. (e) Balsamo, V.; Collins, S.; Hamley, I. W. *Polymer* **2002**, *43*, 4207.
(11) (a) Ge, H.; Hu, Y.; Jiang, X.; Cheng, D.; Yuan, Y.; Bi, H.; Yang, C. *J. Pharm. Sci.* **2002**, *91*, 1463. (b) Hu, Y.; Zhang, L.; Cao, Y.; Ge, H.; Jiang, X.; Yang, C. *Biomacromolecules* **2004**, *5*, 1756.
(12) (a) Lendlein, A.; Schmidt, A. M.; Langer, R. *Proc. Natl. Acad. Sci. U.S.A.* **2001**, *98*, 842. (b) Lendlein, A.; Kelch, S. *Angew. Chem., Int. Ed.* **2002**, *41*, 2034. (c) Jeong, H. M.; Lee, S. Y.; Kim, B. K. *J. Mater. Sci.* **2000**, *35*, 1579. (d) Jeong, H. M.; Kim, B. K.; Choi, Y. J. *Polymer* **2000**, *41*, 1849. (e) Ping, P.; Wang, W.; Chen, X.; Jing, X. *Biomacromolecules* **2005**, *6*, 587.
(13) (a) Jabbari, E.; Wang, S.; Lu, L.; Gruetzmacher, J. A.; Ameenuddin, S.; Hefferan, T. E.; Currier, B. L.; Windebank, A. J.; Yaszemski, M. J. *Biomacromolecules*, in press. (b) Wang, S.; Lu, L.; Gruetzmacher, J. A.; Currier, B. L.; Yaszemski, M. J. *Biomaterials*, in press.

(14) Lide, D. R., Ed.; *Handbook of Chemistry and Physics*, 83rd ed.; CRC Press: Boca Raton, FL, 2002.
(15) Hamdani, M.; Thil, L.; Gans, G.; Feigenbaum, A. E. *J. Appl. Polym. Sci.* **2002**, *83*, 956.
(16) Wang, S.; Lu, L.; Yaszemski, M. J., unpublished results.
(17) Perrin, D. E.; English, J. P. In *Handbook of Biodegradable Polymers*; Domb, A. J., Kost, J., Wiseman, D., Eds.; Harwood Academic Publishers: Amsterdam, 1997; pp 3−27.
(18) Roovers, J.; Toporowski, P. M. *Macromolecules* **1992**, *25*, 3454.
(19) Brandrup, J., Immergut, E. H., Eds.; *Polymer Handbook*, 3rd ed.; Wiley: New York, 1989.
(20) Strobl, G. R. *The Physics of Polymers*, 2nd ed.; Springer-Verlag: Berlin, 1997.
(21) (a) Hobbs, J. K.; Binger, D. R.; Keller, A.; Barham, P. J. *J. Polym. Sci., Part B: Polym. Phys.* **2000**, *38*, 1575. (b) Gazzano, M.; Focarete, M. L.; Riekel, C.; Ripamonti, A.; Scandola, M. *Macromol. Chem. Phys.* **2001**, *202*, 1405.
(22) Wang, Z.; An, L.; Jiang, W.; Wang, X. *J. Polym. Sci., Part B: Polym. Phys.* **1999**, *37*, 2682.
(23) (a) Ong, C. J.; Price, F. P. *J. Polym. Sci., Polym. Commun.* **1978**, *63*, 59. (b) Keith, H. D.; Padden, F. J., Jr.; Russell, T. P. *Macromolecules* **1989**, *22*, 666.
(24) (a) Ma, D.; Luo, X.; Zhang, R.; Toshio, N. *Polymer* **1996**, *37*, 1575. (b) Huang, Y.; Luo, X.; Ma, D. *Eur. Polym. J.* **2001**, *37*, 2153. (c) Ma, D.; Zhang, J.; Wang, M.; Ma, J.; Luo, X. *Macromol. Chem. Phys.* **2001**, *202*, 961. (d) Woo, E. M.; Mandal, T. K.; Lee, S. C. *Colloid Polym. Sci.* **2000**, *278*, 1032.
(25) Keith, H. D.; Padden, F. J., Jr. *Polymer* **1984**, *25*, 28.
(26) Ferry, J. D. *Viscoelastic Properties of Polymers*, 3rd ed.; Wiley: New York, 1980.
(27) (a) Wang, S.; Wang, S.-Q.; Halasa, A.; Hsu, W.-L. *Macromolecules* **2003**, *36*, 5355. (b) Wang, S.; von Meerwall, E. D.; Wang, S.-Q.; Halasa, A.; Hsu, W.-L.; Zhou, J. P.; Quirk, R. P. *Macromolecules* **2004**, *37*, 1641. (c) Wang, S.-Q. *J. Polym. Sci., Part B: Polym. Phys.* **2003**, *41*, 1589. (d) Wang, S.; Elkasabi, Y.; Wang, S.-Q. *Macromolecules* **2005**, *38*, 125.
(28) (a) Roland, C. M.; Ngai, K. L. *Macromolecules* **1992**, *25*, 5765. (b) Roland, C. M.; Ngai, K. L. *Macromolecules* **1996**, *29*, 5747.
(29) Chapman, B. R.; Hamersky, M. W.; Milhaupt, J. M.; Kostelecky, C.; Lodge, T. P.; von Meerwall, E. D.; Smith, S. D. *Macromolecules* **1998**, *31*, 4562.
(30) (a) Santangelo, P. G.; Roland, C. M. *Macromolecules* **1998**, *31*, 4581. (b) Roland, C. M.; Casalini, R. *J. Chem. Phys.* **2003**, *119*, 1838.
(31) Doi, M.; Edwards, S. F. *The Theory of Polymer Dynamics*, 2nd ed.; Clarendon Press: Oxford, England, 1988.
(32) Lodge, T. P.; Rostein, N. A.; Prager, S. *Adv. Chem. Phys.* **1990**, *79*, 1.
(33) Mattice, W. L.; Helfer, C. A.; Sokolov, A. P. *Macromolecules* **2003**, *36*, 9924.
(34) Carella, J. M.; Graessley, W. W.; Fetters, L. J. *Macromolecules* **1984**, *17*, 2775.
(35) Bu, L. J.; Nonidez, W. K.; Mays, J. W.; Tan, N. B. *Macromolecules* **2000**, *33*, 4445.
(36) Perrin, D. E.; English, J. P. In *Handbook of Biodegradable Polymers*; Domb, A. J., Kost, J., Wiseman, D., Eds.; Harwood Academic Publishers: Amsterdam, 1997; pp 63−77.

MA050884C